Check for updates

Effects of different calcium sources on the mineralization and sand curing of CaCO₃ by carbonic anhydrase-producing bacteria

Ling Pan, [ID] [a] Qiongfang Li, [ID] *[ab] Yi Zhou,*[c] Na Song,[a] Lujia Yu,[a] Xuhui Wang,[a] Ke Xiong,[a] LikSen Yap[a] and Jianlin Huo[a]

The deposition and dissolution of calcium carbonate can be affected by the action of biological factors, such as microbial-induced carbonate precipitation (MICP). *Bacillus* spp. has been isolated and applied to prevent soil erosion, increase the stability of slopes, dikes and dunes. However, previous studies have been always limited to a single calcium source ($CaCl_2$) to evaluate the roles of bacteria, and the deposition and curing effect has not yet been quantified. Here, we designed deposition experiments to determine the effect of *Bacillus cereus* with different calcium sources and applied it to sand curing to measure the amount of deposition and curing. The results demonstrated that vaterite was produced when the *Bacillus cereus* participated. Also, more deposition was produced in the $Ca(CH_3COO)_2$ and $CaCl_2$ groups, but the $Ca(NO_3)_2$ group showed optimal curing effects in the sand curing test due to the denser and more uniform deposition. This research will provide an important reference for the design and application of microbial-induced carbonate precipitation.

1 Introduction

$CaCO_3$ is a common mineral and represents the major constituent of the earth's crust, such as in marble and limestone. The deposition of carbonate minerals is observed in organisms such as pearls, shells and bones to rocks and soil. Carbonate precipitation can be directly formed from supersaturated carbonate water or by biological processes, while chemical deposition often occurs with biological factors in the natural environment.[1] Biological factors are indispensable to the special karst landforms and travertine landforms, where the deposition and dissolution of carbonate can be affected by the activities of microbes, and thus can change the structure, morphology and formation.[2,3] Even in extreme environments, such as at the travertine with high temperatures in Yellowstone National Park, USA, the peculiar stromatolite lithofacies were formed by the silica-encrusted cyanobacterial mats.[4,5] In addition, a study in the Arctic thermal spring showed that the formation of rocks is inextricably linked to microbial communities.[6] Many microorganisms can induce the mineralization of $CaCO_3$, but mainly from two groups: carbonic anhydrase- and

urea-producing microorganisms.[7–13] Urease-producing bacteria require urea as a reactant and release NH_3 during biomineralization, which is harmful to human health and the environment ($CO(NH_2)_2 + H_2O \rightarrow NH_2COOH + NH_3$; $NH_2COOH + H_2O \rightarrow NH_3 + H_2CO_3$). Carbonic anhydrase could catalyze the reaction converting CO_2 into HCO_3^- to improve the concentration of CO_3^{2-} and the biomineralization ($CO_2 + H_2O \leftrightarrow HCO_3^- + H^+$; $HCO_3^- \leftrightarrow CO_3^{2-} + H^+$).

Bacillus is a widely distributed genus of bacteria, most strains of which have functions closely related to the microbe-induced carbonate deposition. The study on *Bacillus cereus* isolated from Qatari soils suggested that the aboriginal bacteria could be used to enhance biomineralization in areas where serious erosion has been induced by wind, with an aim to improve the soil stability.[7] Another *Bacillus cereus* strain isolated from the dolomite surfaces of karst topographies had properties yielding CO_2 and carbonic anhydrase (CA) to regulate the concentration of HCO_3^-, thereby inducing the production of $CaCO_3$ crystals.[8] Similarly, Li screened *Bacillus cereus* from a karst soil in Southwest China and studied the biocatalytic precipitation of $CaCO_3$ at different initial concentrations of Ca^{2+} and CA.[9,10] However, the above studies were always limited to a single calcium source ($CaCl_2$) to evaluate the roles of bacteria, while for the purpose of practical application, multiple calcium sources should be involved to decide which reaction condition can be the most suitable for the bacteria strain to function.

Microbial-induced carbonate precipitation (MICP) can increase the deposition of carbonate and produce a calcite crust with high strength.[11,12] It was found that a urease-producing

[a] Life Science and Engineering College, Southwest University of Science and Technology, Mianyang 621010, China. E-mail: liqiongfang1992@126.com; Fax: +86-816-6089521; Tel: +86-816-6089521

[b] Key Laboratory of Solid Waste Treatment and Resource Recycle, Ministry of Education of China, Mianyang 621010, China

[c] School of Agriculture, Food & Wine, Waite Campus, The University of Adelaide, Urrbrae, South Australia, 5064, Australia

bacteria (*Bacillus* sp.) isolated from tropical beach sand was able to form a thin but strong calcite crust with decreased permeability.[13] Moreover, Soon studied the curing effects of MICP on tropical residual soil and sand using *Bacillus megaterium*, and found a significant improvement in shearing strength and anti-permeability from the bacteria treatment.[14] However, the deposition of calcium carbonate and the hardness of the calcite crust formed by the bacteria have not been quantitatively determined yet, hence a comparison of the efficiency between different bacteria strains for forming calcium carbonate is impossible.

Recently, we isolated a dominant bacteria strain from Huanglong, identified as *Bacillus cereus*. The experimental microbes in previous biomineralization studies were mostly derived from rocks or soils in plain or high mountain areas, and the temperature and humidity of the growth environment were basically at a medium level; however, the Huanglong scenic in Sichuan, China, is located in the eastern part of the Qinghai-Tibet Plateau. Here, a large amount of cold-water travertine was formed with the perennially low temperature (4 °C) and at a high elevation (3145–3578 m).[15] Studies on the travertine in Huanglong have shown that the biodiversity of bacteria and algae is significantly high, and the water contains a large amount of Ca^{2+}, Mg^{2+} and HCO_3^-, thus forming an unique travertine landform and cold adaption condition.[16] Hence, a study of aboriginal bacteria in Huanglong can provide reference for the research and application of biomineralization in a low temperature environment.

The objectives of this study were: (1) to evaluate the *Bacillus cereus*-induced carbonate precipitation under different calcium sources ($CaCl_2$, $Ca(NO_3)_2$ and $Ca(CH_3COO)_2$); (2) to quantify the deposition amount and shear strength of a treated sand column.

2 Materials and methods

2.1 Bacterial strain

Experimental bacteria (*Bacillus cereus*) were provided by the Microbiology Laboratory of Southwest University of Science and Technology, with this indigenous bacteria strain isolated from travertine pool water in Huanglong, which has been demonstrated to possess the property of carbonic anhydrase production.[17] The bacteria were incubated for 24 h in a beef extract peptone medium (per 1000 mL of a medium containing beef extract 3.0 g, peptone 10.0 g, NaCl 5.0 g and deionized water 1000 mL, pH 7.4–7.6), with the condition of 30 °C, 120 rpm shaking incubator cultivation.

2.2 Preparation of the deposition systems

Each system contained 100 mL $NaHCO_3$ (0.15 M), and the calcium sources were $CaCl_2$, $Ca(NO_3)_2$ and $Ca(CH_3COO)_2$, respectively. The bacterial seed was inoculated into the liquid medium at a 1% inoculation ratio as the experimental group. The control group had the same volume of sterilized liquid medium. The total volume of the deposition system was 300 mL. The composition of each system is shown in Table 1. Each

system was mineralized in a conical flask under the condition of 25 °C, 120 rpm, and the experiment lasted for 72 h.

2.3 Characterization

The pH and conductivity of each system were monitored using a pH meter (PHS-320) and conductivity meter (DDS-307) every 3 h for the first 12 h, and every 12 h after that. The supernatant was discarded, and the sediment was thoroughly washed with deionized water after the deposition. The total weight (M_0) of the bottle and sediment after drying (60 °C) were recorded. Then, we scraped out the deposition, cleaned the bottle, and weighed the empty bottle (M_1) after drying. The amount of deposition was calculated by subtraction ($M_0 - M_1$), and the dried deposition was used in the subsequent tests.[18]

X-ray diffraction (XRD, D/max2200VPC, Japan) was performed to identify the crystalline phases of the deposition, with the condition of a diffraction angle (2θ) 3°–80° at a scan rate of 0.1° min^{-1}. The functional groups of the deposition were determined on a Fourier-transform infrared spectrometer (FT-IR, Nico-let 5700, USA). The samples were scanned from 4000 to 400 cm^{-1} with a resolution of 0.4 cm^{-1}. We ground the dried deposition into powder and characterized the microstructure *via* scanning electron microscopy (SEM, Carl Zeiss NTS GmbH UItra5, Germany).[19]

2.4 Preparation for the sand-curing experiment

Geotextile possesses a property of good permeability and shaping, so it was selected as the mould material (400 g m^{-2}, Shandong Jiantong Geosynthetics Co., Ltd.). We cropped the geotextile into pieces of a suitable shape and size and sewed them into a cylindrical shape with a diameter of 60 mm and a height of 50 mm. Xiamen ISO standard sand (particle size 0.28–0.85 mm) were used in this experiment.[20] We soaked the sand with 1 M HCl until there were no bubbles generated, then washed it repeatedly with deionized water 4–5 times and finally dried it.

We loaded the sands into each geotextile mould with the same weight (150 g), and then, injected the microbial reaction mixture into the sand column using a plastic dropper. The microbial reaction mixture was the same as the deposition experiment. Grouting was performed once a day for seven days, 25 mL each time. After completing the experiment, demoulding the sand column and then drying it at 60 °C, the shear strength was measured using a strain-controlled direct shear tester (ZJ-2). The weight of specimen in each group was weighed (M_0)

Table 1 Composition of each deposition systems

Group	1	2	3	4	5	6
$NaHCO_3$ (mL)	100	100	100	100	100	100
$CaCl_2$ (mL)	100	100	0	0	0	0
$Ca(NO_3)_2$ (mL)	0	0	100	100	0	0
$Ca(CH_3COO)_2$ (mL)	0	0	0	0	100	100
Bacteria solution (mL)	100	0	100	0	100	0
Sterilizing medium (mL)	0	100	0	100	0	100

after a complete curing test. Then, we washed the specimen with 1 M hydrochloric acid and ultrapure water after the shearing test, until there were no bubbles generated, and weighed it after drying (M_1). The amount of deposition generated by the cured process was obtained by the method of subtraction.[21]

3 Results and discussion

3.1 pH and conductivity

The variations in pH and conductivity during the deposition process are shown in Fig. 1. In the first 3 h, the pH and conductivity decreased sharply with the chemical deposition (Fig. 1A). Ca^{2+} and CO_3^{2-} combined rapidly to form $CaCO_3$, and the consumption of CO_3^{2-} promoted the ionization of HCO_3^-, and thus accelerated the chemical deposition. H^+ in the solution rapidly increased because of the consumption of CO_3^{2-}, which resulted in a significant decline in the pH value. Then, the chemical reaction was basically in equilibrium.

The pH of the experimental groups fluctuated more significantly than that of the control groups of $Ca(NO_3)_2$ and $CaCl_2$ due to the supplementation of bacteria.[22] However, the fluctuation of pH in the $Ca(CH_3COO)_2$ control group was clearly comparable to the $Ca(NO_3)_2$ and $CaCl_2$ ones. This might have been due

to the reversible ionization of the weak electrolyte (CH_3COOH → CH_3COO^- + H^+);[23] hence, the pH in the $Ca(CH_3COO)_2$ control group was more sensitive to the change in ions in the system. In addition, although the experiment was performed at a constant temperature, since the incubator shaker was opened for each test, this could have possibly led to a temperature change and also the instability of the test results. The pH and conductivity of the experimental groups were all higher than those for the control group. It was speculated that the metabolism of bacteria increased the pH of the experimental groups. It seems that while the controls became stable, the pH of the experimental groups still fluctuated greatly at the end of the experiment. Hence, it was possible that the pH value would rise again after 72 h. It is known that microorganisms are rich in metabolites, and many of the complex compounds produced through the metabolic pathways could influence the pH of the solution, and thus the biomineralization of $CaCO_3$ could be affected.[24–26]

3.2 Deposition amount

The amount of $CaCO_3$ precipitated in each system is shown in Fig. 2. More deposition was produced in the experimental groups as compared to the control groups of $Ca(CH_3COO)_2$ and $CaCl_2$, suggesting the presence of bacteria increased the production of deposition when $Ca(CH_3COO)_2$ and $CaCl_2$ were provided as the calcium sources. The nucleation site is one of the main factors for calcium carbonate precipitation, whose availability significantly increased in the presence of bacteria, as the bacterial cells or their metabolites could serve as a nucleation site for the precipitation reaction.[27,28] The pH of each system changed greatly with the addition of the initial reactants in practice, and the loss of CO_2 occurred during the process, which was hard to quantify. The $Ca(CH_3COO)_2$ group has weak acidity compared with $Ca(NO_3)_2$ and $CaCl_2$, which was associated with its higher pH value from Fig. 1. Therefore, less CO_2 was lost and more deposition was produced in the
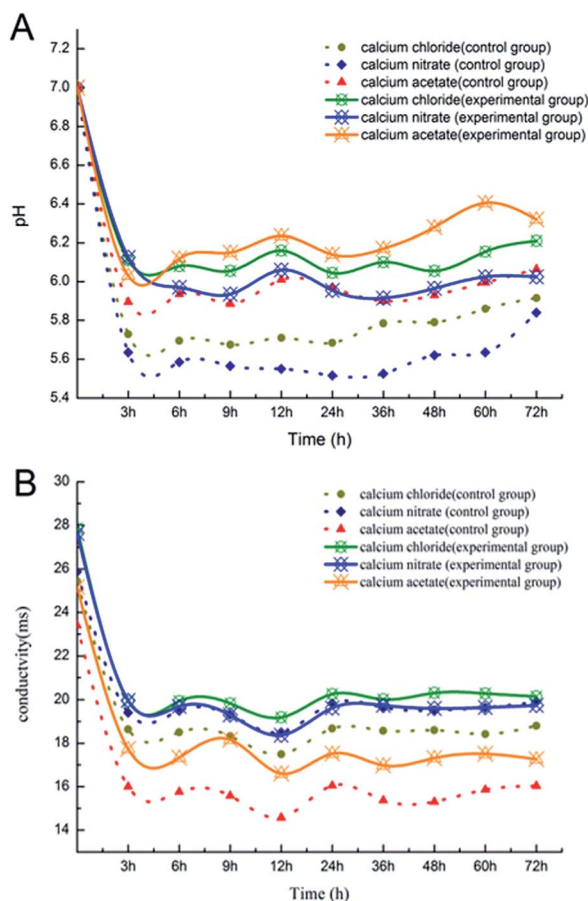

Fig. 1 (A) The change in pH during the deposition process; (B) the change in electric conductivity during the deposition process.
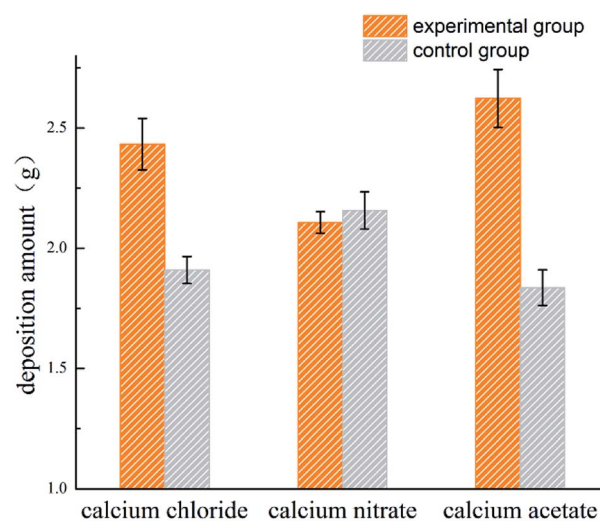

Fig. 2 The deposition amount of the three different calcium sources.

$Ca(CH_3COO)_2$ group, which enhanced the utilization of CO_2 by the experimental bacteria.[29] In addition, $CaCO_3$ deposition was inevitable in all systems because of the supersaturated environment. Nevertheless, the deposition systems of the inoculated and uninoculated bacteria were used, and they showed comparable deposition amounts.

3.3 Morphological observation and crystal characterization

The FT-IR spectra for the $CaCO_3$ crystals produced during deposition are shown in Fig. 3. The characteristic peaks of calcite were at 712 cm^{-1}, 875 cm^{-1} and 2515 cm^{-1} for all the systems, which indicated that calcite was the most predominant polymorphs produced in each system.

However, a combination of vaterite and calcite was induced when the bacteria were added to the deposition systems (Fig. 4), and the peaks at 1087 cm^{-1} and 744 cm^{-1} were the characteristic peaks of vaterite. Besides, there were also some other absorptions that peaked at 3430 cm^{-1}, 2950–2850 cm^{-1}, 2500 cm^{-1}, 1750 cm^{-1}, and 1450 cm^{-1}, which mainly generated due to the vibration of the O–H, C–H and N–H groups in the water and organics. These organic functional groups were potentially derived from the culture medium or *Bacillus cereus* bacteria. However, new crystalline polymorphs were generated only in the experimental groups. Therefore, the vaterite produced in the deposition was not due to the culture medium

but rather due to the metabolic activity of *Bacillus cereus*. In addition, the morphology of minerals can also be affected by some specific organic functional groups.[30,31]

To determine the mineral phases, we characterized the $CaCO_3$ crystals produced in each system *via* XRD. The diffraction angles (2θ) of the deposition in the calcium acetate experiment group were 22.9°, 24.8°, 27.0°, 29.3°, 31.3°, 32.7°, 35.9°, 39.3°, 43.0°, 47.3°, and 48.4°, corresponding to the (*hkl*) indices (012), (100), (101), (104), (006), (102), (110), (113), (202), (018), and (116) (Fig. 4). In the control group without the biological factor, the diffraction angles (2θ) were 23.0°, 29.3°, 31.4°, 35.9°, 39.3°, 43.1°, 47.4°, and 48.4°, corresponding to the (*hkl*) indices (012), (104), (006), (110), (113), (202), (018) and (116). According to the diffraction angles (2θ) 24.8°, 27.0° and 32.7°, corresponding to the (*hkl*) indices (100), (101) and (102), both calcite and vaterite were produced with the bacteria, rather than calcite only in the control groups, which is consistent with the FT-IR analysis. The result was similar to that of the calcium chloride and calcium nitrate groups, and a comparison of the three experimental groups revealed that the calcium acetate group with bacteria induced a higher portion of vaterite than the calcium chloride and calcium nitrate groups. These data indicated that the presence of *Bacillus cereus* prompted the precipitation of vaterite particles. Previous studies have demonstrated that the bioprecipitation of $CaCO_3$ may result in the production
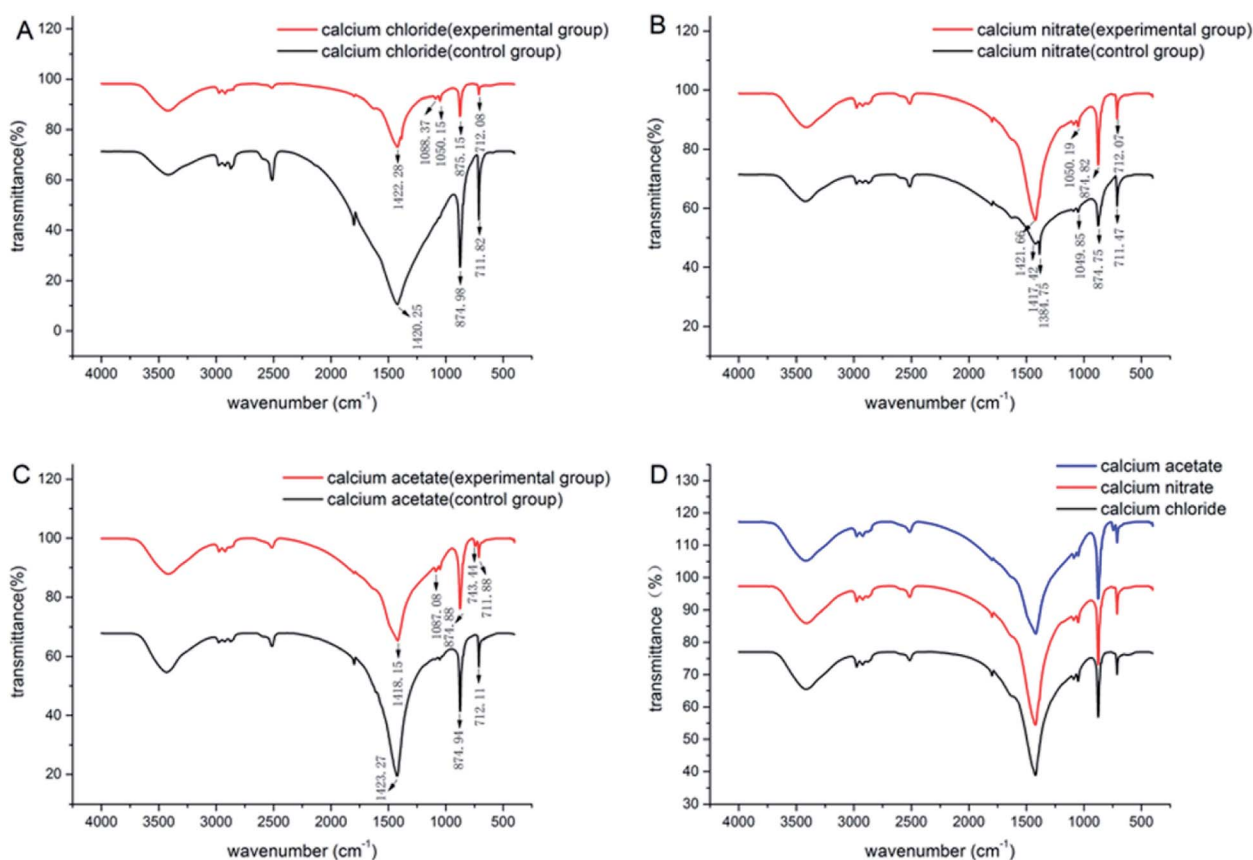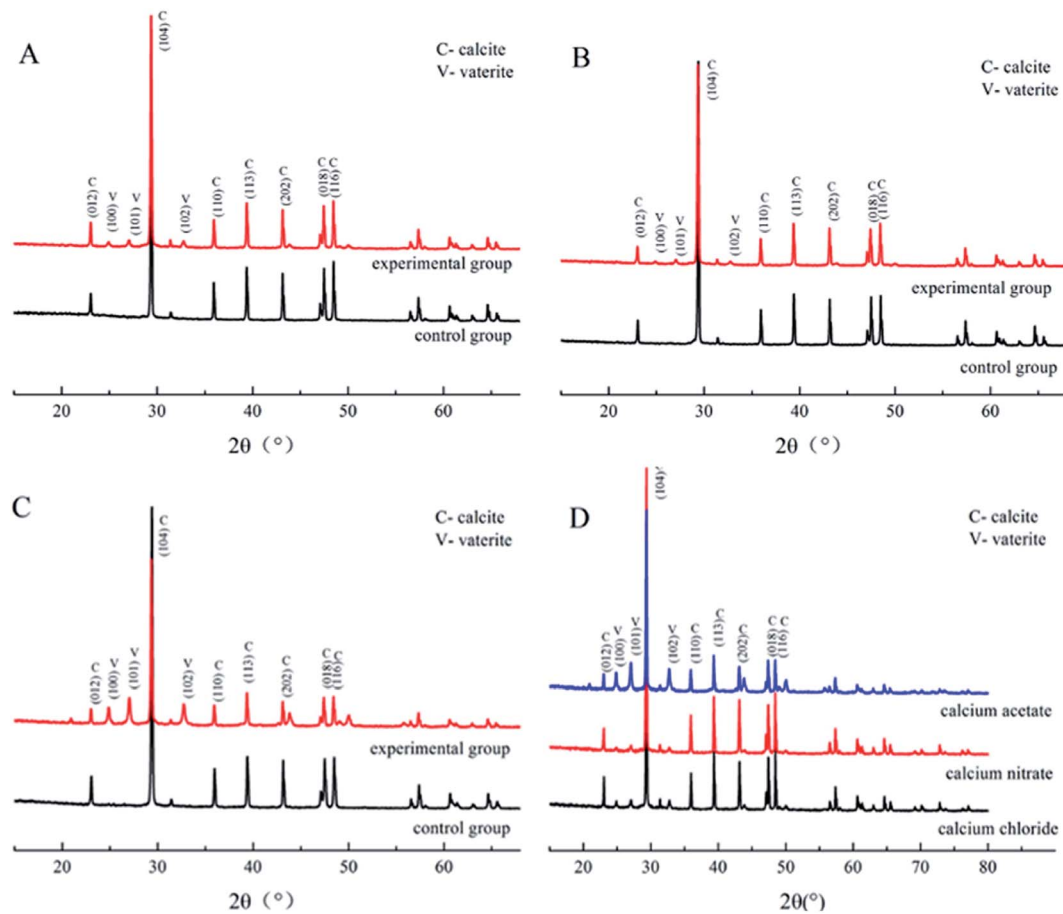

Fig. 3 IR patterns of $CaCO_3$ formed with the three different calcium sources: (A) $CaCl_2$ system; (B) $Ca(NO_3)_2$ system; (C) $Ca(CH_3COO)_2$ system; (D) comparison of the three experimental groups.

Fig. 4 XRD patterns of CaCO₃ formed with the three different calcium sources: (A) CaCl₂ system; (B) Ca(NO₃)₂ system; (C) Ca(CH₃COO)₂ system; (D) comparison of the three experimental groups.

of different polymorphs, including calcite, vaterite, aragonite, and ikaite.[32,33] The bacterial extracellular polymeric substance (EPS) is the key factor influencing the morphology of the precipitated particles,[34] which generally possess the property of metal binding, such as Ca^{2+}, as its high molecular weight compounds with charged functional groups.[35] Besides, it is also affected by complex enzymatic systems, such as a diverse range of EPS, and enzymes, including protein, nucleic acid, and polysaccharides, that are produced *via* the metabolic activities of bacteria. Furthermore, many of the biomineralization-related substances have common characteristics, such as highly glycosylated, acidic,[36,37] and anionic functional groups.[38,39] These differences between the control and experimental groups were due to the presence of the bacteria. In addition, the complex interactions between EPS and inorganic ions also affected the deposition.

The crystal shapes of CaCO₃ particles in each system were distinguishable by SEM. The majority of the crystals precipitated in the control groups were basically the same, mainly square or rhombohedral with overlaps and an irregular structure (Fig. 5A, D and G). While the bioprecipitation of CaCO₃ may result in different polymorphs,[40] it was visually confirmed that different shapes of crystals were precipitated. With the effect of the bacteria in the experimental groups, the crystal morphology

was significantly changed both in the CaCl₂ and Ca(CH₃COO)₂ groups. It could be seen that raspberry-shaped crystals were generated in the CaCl₂ system. Plenty of spherical crystals were
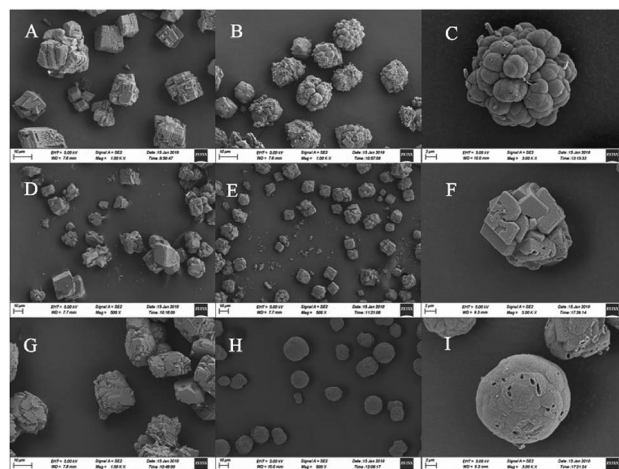

Fig. 5 The morphology of CaCO₃ formed with the three different calcium sources in the presence of *Bacillus cereus* (+) or not (−): (A) CaCl₂ system (−); (B) CaCl₂ system (+); (D) Ca(NO₃)₂ system (−); (E) Ca(NO₃)₂ system (+); (G) Ca(CH₃COO)₂ system (−); (H) Ca(CH₃COO)₂ system (+); (C), (F) and (I) are the high magnifications of (B), (E) and (H).

seen clearly in the Ca(CH₃COO)₂ experimental group, and the surface was relatively flat and smooth (Fig. 5H), and a large number of holes of bacterial activity were visualized on the surface or interior of the crystals (Fig. 5C, F and I). It is worth noting that the size of particles in the control group of Ca(NO₃)₂ were generally between 10–40 μm, while the size of particles was mainly 15–20 μm when the bacteria were added (Fig. 5E). The uniform and smaller size contributed to the enhancement of the effectiveness of cracks remediation and sand cohesiveness.[41] In our investigation, the results obtained by FT-IR and XRD disclosed that the vaterite formation was facilitated with the presence of *Bacillus cereus* and its metabolites. Besides, it also had an effect on the CaCO₃ morphology, which can be seen clearly in Fig. 5.

3.4 External morphology of the sand-cured specimen

The cured samples in the CaCl₂ group and the Ca(NO₃)₂ group were well formed. The sand column remained a regular and smooth cylindrical shape without any loose sand scattered around, and the surface tended to be brown-yellow (Fig. 6A and B). While the cured samples in the Ca(CH₃COO)₂ group were not fully formed, with sand grains falling around and with an incomplete shape and yellow-white surface (Fig. 6C). It is remarkable that there were holes on the surface of each specimen, which was likely because of CO_2 hydration catalyzed by carbon anhydrase, producing CO_2 continuously during that process, thus leaving holes on the surface of these specimens. The sand column without any treatment could not be cured to a whole block, and thus they were still loose sands without any strength after demoulding. After the shearing test, the upper and lower parts of the sample in the Ca(NO₃)₂ and CaCl₂ groups were fragmented (Fig. 6G and H), while those in the Ca(CH₃-COO)₂ group were sanded (Fig. 6I). This suggested that the Ca(NO₃)₂ group had the best curing effect with the presence of the experimental bacteria.

3.5 Deposition and shearing strength

The amount of CaCO₃ from the different calcium sources deposited during the curing process was different. The Ca(CH₃COO)₂ group possessed the largest deposition amount, while the difference between the CaCl₂ group and Ca(NO₃)₂ group was not significant, which is basically consistent with the results from the deposition experiment. The relationship between the shear stress and displacement is shown in Fig. 7A. With the effect of the experimental bacteria, the sand was cured into a whole sand column, but the curing effect was different. Among the three calcium sources selected in this experiment, the sand column of the Ca(NO₃)₂ group had the highest shearing strength (62.33 kPa), followed by the CaCl₂ group, while the Ca(CH₃COO)₂ group had the worst curing effect (only 11.19 kPa).

The calcite crystals produced by the CaCl₂ and CaNO₃ systems were combined closely and well distributed (Fig. 9A and C), which were clustered to the sand particles to improve the cementation of sands, and also enhanced the cured strength of the column. Conversely, calcite crystals from the Ca(CH₃COO)₂ systems were inhomogeneous and most of them were scattered
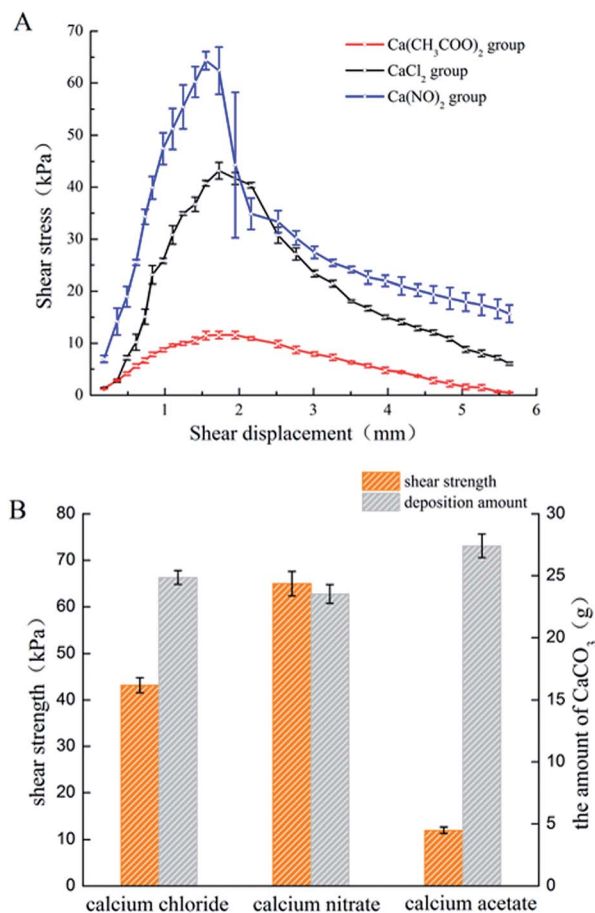

Fig. 7 (A) The shear stress and displacement chart of the sand column with the three different calcium sources; (B) the shear strength and the deposition amount of the sand column with the three different calcium sources.

Fig. 6 The shape of the sand column under the three different calcium sources with the effect of *Bacillus cereus*: (A and D) CaCl₂ group; (B and E) Ca(NO)₂ group; (C and F) Ca(CH₃COO)₂ group; (G) CaCl₂ group after shearing; (H) Ca(NO₃)₂ group after shearing; (I) Ca(CH₃COO)₂ group after.
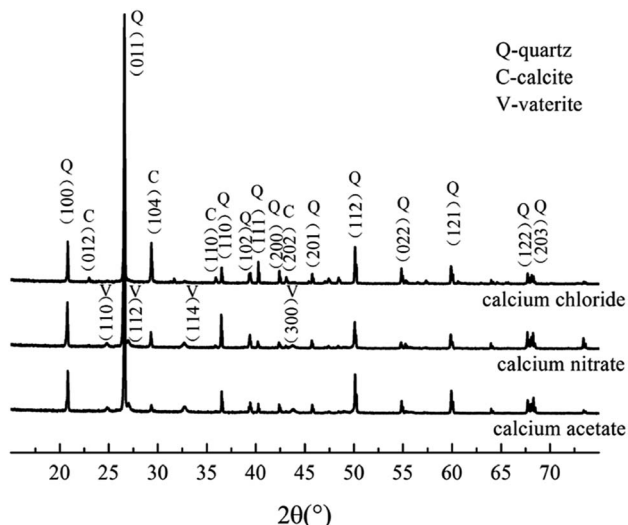
Fig. 8 XRD pattern of the three experimental groups.

around the sand, instead of attached to the surface of the sand (Fig. 9E), which presented a lower shearing strength.[42] In addition, the crystals on the surface of the sand in the $Ca(NO_3)_2$ and $CaCl_2$ groups were denser than that of $Ca(CH_3COO)_2$, which was the key factor that reduced the adhesion between sands and also the shearing strength.[43] XRD results showed the crystal type and its approximate content. The diffraction of vaterite observed in the calcium acetate group was more obvious than in the other two groups, but the evidence of calcite was limited

Fig. 9 SEM images of sand and $CaCO_3$ formed in the sand columns: (A and B) $CaCl_2$ group; (C and D) $Ca(NO_3)_2$ group; (E and F) $Ca(CH_3COO)_2$ group.

(Fig. 8), which is unfavourable to the curing of sands.[44,45] In addition, there was a large difference in the size of particles in the calcium acetate group, which was generally between 10–30 μm. However, the size of particles was mainly 10–15 μm in the other two groups (Fig. 5), which may be the reason for the difference in shearing strength.[41] Although the largest amount of deposition was produced in the $Ca(CH_3COO)_2$ system, most of them were unable to bond the sand particles, which we termed as a non-effective connection.[46] These results suggested that a good uniform calcite distribution and size contributed to enhancing the effectiveness of the shearing strength.

4 Conclusion

The current study showed that the presence of *Bacillus cereus* strain increased the pH of deposition systems, and also increased the amount of deposition when $Ca(CH_3COO)_2$ and $CaCl_2$ were provided as the calcium sources. The formation of vaterite was promoted with the effect of *Bacillus cereus* in experimental groups, especially in the $Ca(CH_3COO)_2$ system. In addition, the deposition formed by the $Ca(NO_3)_2$ system in the sand-curing experiment was denser and more uniform, which is favourable to sand curing. Hence, the sand column in the $Ca(NO_3)_2$ system possessed the highest shearing strength.

Conflicts of interest

There are no conflicts to declare.

Acknowledgements

Notes and references

1 M. Ghobadi and R. Babazadeh, *Rock Mech. Rock Eng.*, 2014, **48**(3), 1001–1016.
2 C. Glunk, C. Dupraz, O. Braissant, K. Gallagher, E. Verrecchia and P. Visscher, *Sedimentology*, 2011, **58**(3), 720–738.
3 C. Bayari, *Earth Surf. Processes Landforms*, 2002, **27**(6), 577–590.
4 C. Ranney, W. Berelson, F. Corsetti, M. Treants and J. Spear, *Environ. Microbiol.*, 2012, **14**(5), 1182–1197.
5 J. Kim, T. Kogure, K. Yang, S. Kim, Y. Jang, H. Baik and G. Geesey, *Clays Clay Miner.*, 2012, **60**(5), 484–495.
6 V. Starke, J. Kirshtein, M. Fogel and A. Steele, *Environ. Microbiol. Rep.*, 2013, **5**(5), 648–659.
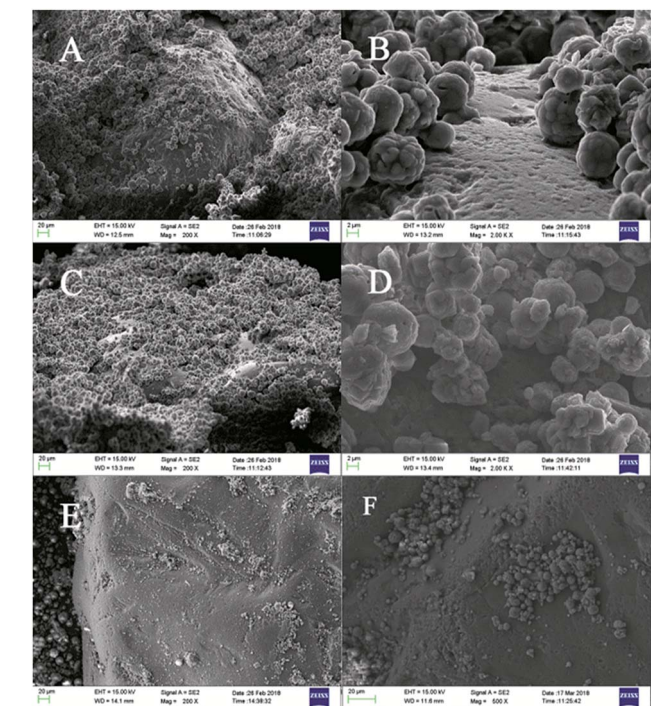7 S. Bibi, M. Oualha, M. Ashfaq, M. Suleiman and N. Zouari, *RSC Adv.*, 2018, **8**, 5854–5863.

8 J. Han, B. Lian and H. Ling, *Geomicrobiol. J.*, 2013, **30**(8), 682–689.

9 W. Li, W. Chen, P. Zhou, S. Zhu and L. Yu, *Chem. Eng. J.*, 2013, **218**, 65–72.

10 W. Li, W. Chen, P. Zhou and L. Yu, *Chem. Eng. J.*, 2013, **232**, 149–156.

11 L. Cheng, M. Shahin, R. Cordruwisch, M. Addis, T. Hartanto and C. Elms, *7th International Congress on Environmental Geotechnics*, 2014, pp. 1105–1112.

12 R. Tarczewski, *Procedia Manuf.*, 2015, **3**, 1704–1711.

13 J. Chu, V. Stabnikov and V. Ivanov, *Geomicrobiol. J.*, 2012, **29**(6), 544–549.

14 N. Soon, L. Lee, T. Khun and H. Ling, *KSCE J. Civ. Eng.*, 2013, **17**(4), 718–728.

15 Q. Li, F. Dong, Q. Dai, T. Huo, D. An and S. Tang, *Adv. Mater. Res.*, 2012, **518**, 136–139.

16 S. Sun, F. Dong, H. Ehrlich, X. Zhao, M. Liu, Q. Dai, Q. Li, D. An and H. Dong, *Int J Environ Res Public Health*, 2014, **11**(12), 13084–13096.

17 Q. Yang, X. He, Q. Li, L. Yu, X. Wang and L. Pan, *Ind. Constr.*, 2018, **48**(7), 38–43.

18 S. Katsev and M. Dittrich, *Ecol. Model.*, 2013, **251**, 246–259.

19 X. Jiang, Q. Lin, M. Zhang, G. He and Z. Sun, *Nanoscale Res. Lett.*, 2015, **10**(1), 1–6.

20 A. Jotisankasa and N. Rurgchaisri, *Geotext. Geomembranes*, 2018, **46**(3), 338–353.

21 H. Eid, R. Amarasinghe, K. Rabie and D. Wijewickreme, *Can. Geotech. J.*, 2015, **52**(2), 198–210.

22 B. Mortensen, M. Haber, J. Dejong, L. Caslake and D. Nelson, *J. Appl. Microbiol.*, 2011, **111**(2), 338–349.

23 S. Fisher, A. Kovalevsky, J. Domsic, M. Mustyakimov, D. Silverman, R. Mckenna and P. Langan, *Acta Crystallogr. D*, 2010, **66**(11), 1178–1183.

24 G. Falini, M. Reggi, S. Fermani, F. Sparla, S. Goffredo, Z. Dubinsky, O. Levi, Y. Dauphin and J. Cuif, *J. Struct. Biol.*, 2013, **183**(2), 226–238.

25 M. Kiran, K. Pakshirajan and G. Das, *Chem. Eng. Sci.*, 2017, **158**, 606–620.

26 L. Ren, Z. Hong, W. Qian, J. Li and R. Xu, *Environ. Pollut.*, 2018, **237**, 39–49.

27 G. Long, P. Zhu, Y. Shen and M. Tong, *Environ. Sci. Technol.*, 2009, **43**(7), 2308–2314.

28 M. Obst, J. Dynes, J. Lawrence, G. Swerhone, K. Benzerara, C. Karunakaran, K. Kaznatcheev, T. Tyliszczak and A. Hitchcock, *Geochim. Cosmochim. Acta*, 2009, **73**(14), 4180–4198.

29 M. Edman and A. Omstedt, *Limnol. Oceanogr.*, 2012, **58**(1), 74–92.

30 C. Glunk, C. Dupraz, O. Braissant, K. Gallagher, E. Verrecchia and P. Visscher, *Sedimentology*, 2010, **58**(3), 720–736.

31 J. Aizenberg, G. Lambert, S. Weiner and L. Addadi, *J. Am. Chem. Soc.*, 2002, **124**(1), 32–39.

32 N. Dhami, M. Reddy and A. Mukherjee, *J. Microbiol. Biotechnol.*, 2013, **23**(5), 707–714.

33 R. Sevcik, P. Sasek and A. Viani, *J. Mater. Sci.*, 2017, **53**(6), 4022–4033.

34 M. Seifan, A. Samani and A. Berenjian, *Appl. Microbiol. Biotechnol.*, 2016, **100**(23), 9895–9906.

35 P. Bhaskar and N. Bhosle, *Environ. Int.*, 2006, **32**(2), 191–198.

36 N. Wada, K. Kanamura and T. Umegaki, *J. Colloid Interface Sci.*, 2001, **233**(1), 65–72.

37 H. Wang, C. Bocker, B. Li, H. Lin, R. Christian and L. Luo, *Solid State Sci.*, 2017, **70**, 6–12.

38 M. Suzuki, K. Saruwatari, T. Kogure, Y. Yamamoto, T. Nishimura, T. Kato and H. Nagasawa, *Science*, 2009, **325**(5946), 1388–1390.

39 S. Collino and J. Evans, *Biomacromolecules*, 2008, **9**(7), 1909–1918.

40 M. Seifan, A. Samani, S. Hewitt and A. Berenjian, *Fermentation*, 2017, **3**(4), 57.

41 M. Seifan and A. Berenjian, *World J. Microbiol. Biotechnol.*, 2018, **34**(11), 168.

42 X. Wang, W. Guo, F. Yu, Z. Yi and L. Sun, *Rock Soil Mech.*, 2016, **37**(2), 363–368.

43 K. Andersen and K. Schjetne, *J. Geotech. Geoenviron. Eng.*, 2013, **139**(7), 1140–1155.

44 M. Cui, J. Zheng, R. Zhang, H. Lai and J. Zhang, *Acta Geotech.*, 2017, **12**(5), 971–986.

45 H. Son, H. Kim, S. Park and H. Lee, *Materials*, 2018, **11**(5), 782.

46 Y. Zhang, H. Guo and X. Cheng, *Constr. Build. Mater.*, 2015, **77**, 160–167.